JEE Journal of Ecological Engineering

*Journal of Ecological Engineering*, 2026, 27(9), 173–184
https://doi.org/10.12911/22998993/221452
ISSN 2299–8993, License CC-BY 4.0

Received: 2026.04.05
Accepted: 2026.07.15
Published: 2026.08.01

# Impact of pavement design on albedo: A strategy to mitigate the urban heat island

Roberto Angeles Vasquez[1*], Julio Miguel Angeles-Suazo[2], Pabel Mariano Meza Mitma[2], Jairo Edson Gutiérrez-Collao[2], Leticia Leiva Arauco[3], Fernando Boza Ccora[1], Rosa Zarate Quiñones[3], Nataly Angeles-Suazo[4], Hugo Abi Karam[5]

[1] Facultad de Ingeniería Civil, Universidad Nacional del Centro del Perú, Huancayo, Peru
[2] Escuela Profesional de Ingeniería Forestal y Ambiental, Universidad Nacional Autónoma de Tayacaja Daniel Hernández Morillo, Tayacaja, Peru
[3] Unidad de Posgrado, Facultad de Ciencias Forestales y del Ambiente, Universidad Nacional del Centro del Perú, Av. Mariscal Ramón Castilla 3909, Tambo, Peru
[4] Universidad Tecnológica del Perú, Huancayo, Peru
[5] Universidade Federal do Rio de Janeiro, Rio de Janeiro, Brazil
* Corresponding author's e-mail: rangeles@uncp.edu.pe

## ABSTRACT

The urban heat island (UHI) effect is intensified by the thermal properties and low reflectance of conventional pavement materials, with Huancayo being a city with high urban temperatures. Permeable concrete (PC) is therefore presented as an alternative to improve urban quality of life. The objective of this study is to evaluate the effect of the proportions and factorial interaction of aggregate size, color, and plasticizer additive on the thermal conductivity, thermal resistance, and surface albedo of PC. A factorial design (3 levels of factor Size of coarse aggregate x5 levels of factor Color of concrete x 2 levels of factor Plasticizer additive with 3 repetitions) with three replicates was used, with a total of 90 PC test specimens; the Thermtest TLS–100 and a pyranometer were used to evaluate the parameters. The results showed that thermal conductivity was not very sensitive to the factors evaluated, and no statistically significant effects were found. On the other hand, thermal resistance did show significant effects related to the color of the concrete and its interaction with the plasticizer additive. Albedo proved to be the most sensitive variable, where color and its interactions with aggregate size and additive had a notable impact on surface reflectance, with light colors showing the highest values. The design of the PC mixture can affect its thermal and optical performance. This highlights its potential as a strategy to reduce heat absorption and help mitigate the UHI effect. Future research should analyze the behavior of PC in real field conditions, taking into account factors such as humidity, evaporation, material aging, and the use of pigments or reflective additives.

**Keywords:** pervious concrete, urban heat island, reflectance.

## INTRODUCTION

Urbanized areas tend to have different climates depending on their urban and rural areas. This phenomenon is known as the urban heat island (UHI) (Van, 2025) and includes variations in air temperature and land surface temperature (LST) (Xiang et al., 2023). Thus, there are two common phenomena, but they are not the only ones: i) surface urban heat island (SUHI), which refers to the difference in surface temperature between urban and rural areas, measured by remote sensing (satellite or aerial) (Ahmed, 2018) and ii) canopy urban heat island (CUHI), which comprises the air temperature from the ground to the tops of buildings and trees, measured from terrestrial weather stations (Bechtel et al., 2019; Venter et al., 2021). In addition, a computational fluid dynamics (CFD) model shows that during the dry season, the highest surface temperature in an urban microclimate is located in the center of a canyon between buildings, while convective heat flow is stored between sunrise and sunset, being released into the environment with a direct influence from wind speed, rainfall, solar radiation, and urban materials (Kubilay et al., 2018).

Urbanization, as one of the factors contributing to the UHI, causes a decrease in green areas, a change in surface reflectivity, and an increase in impervious surfaces (Cimolai and Aguilar, 2025); which, together with landscape and topographic characteristics, affect urban heat exchange processes (Mirabi and Davies, 2022; Sharifi, 2019; Wang et al., 2021). Its effects exacerbate morbidity and mortality problems due to heat–related illnesses, posing a risk to public health (Cleland et al., 2023); in addition, increased use of air conditioning leads to greenhouse gas emissions (Lai et al., 2019). In the case of Huancayo, the increase in conventional concrete paving and construction is causing a progressive increase in the SUHI, with considerably high daytime and nighttime values (S. J. Angeles et al., 2019; V. R. Angeles et al., 2024).

In this regard, the physical characteristics of urban infrastructure materials contribute to high urban temperatures, taking into account their capacity to absorb sunlight. For example, asphalt absorbs too much and reflects too little, storing large amounts of heat during the day and slowly releasing it at night (Joshi et al., 2025). In addition, pavement covers around 20–40% of urban surfaces, with 75–80% of roads being asphalted (Sankar et al., 2021). In tropical and semi-arid climates, conventional asphalt and concrete pavements reflect 10–30%, depending on environmental exposure and aging (Abedrabboh et al., 2025); so their thermal properties (thermal conductivity, reflectivity, and heat storage) influence the intensity of the UHI (Liu et al., 2019). In environments with strong solar incidence, pavement temperatures can reach up to 60 °C and even higher at midday (Sankar et al., 2021).

In recent decades, changing urban geometry, planting vegetation, and incorporating bodies of water have been used as strategies to improve urban temperature (Bai and Xing, 2025; Tun et al., 2025), but they have not been implemented on a large scale due to political, technical, and economic constraints. However, it is necessary to implement UHI mitigation strategies and increase the albedo of the urban surface, for example, by using reflective materials to minimize heat absorption and storage, taking into account the local characteristics of the urban microclimate (Rahmani and Sharifi, 2025), as Huancayo is a city with an increase in local surface temperature due to the UHI (V. R. Angeles et al., 2024).

Thus, permeable concrete (PC), due to its porous structure (aggregate of a single grain size and a binder), offers a double benefit as it manages stormwater through its porous matrix and reduces the effects of UHI compared to conventional concrete (Y. Liu et al., 2020). The composition of PC consists of a cement content of 280 to 310 kg/m$^3$ (Alighardashi et al., 2018), aggregates ranging from 1440 to 1800 kg/m$^3$ (AlShareedah, 2020; Chandrappa and Biligiri, 2016; Eisenberg et al., 2015), a water–cement ratio of 0.26–0.45 (Kevern et al., 2009) and aggregate-cement ratio of 4:1–4.5:1 (Tyson and Tayabji, 2012). However, these values may not be universal, as the optimal mixture depends on the understanding of the individual properties of each component, as well as structural and environmental requirements (Mostafa et al., 2024). In addition, in order to implement PC as a measure to mitigate the effects of UHI, studies on thermal properties and reflectivity or albedo are required, since the amount of solar absorption depends on the product of solar irradiance and albedo (Lu et al., 2023).

Therefore, the objective of this study is to evaluate the effect of the proportions and factorial interaction of aggregate size, color, and plasticizer additive on the thermal conductivity, thermal resistance, and surface albedo of modified (porous) PC, compared to conventional concrete, as a strategy for mitigating the UHI in paved roads in the city of Huancayo, Peru.

## MATERIALS AND METHODS

### Location

The experimental tests on the PC were carried out at the National University of Central Peru (UNCP), in the concrete laboratory of the Faculty of Civil Engineering, located in the district of "El Tambo," province of Huancayo, department of Junín, at 12° 01' 56.58'' S and 75° 14' 06.91'' W, in the Central Andes of Peru (Figure 1).

### Components of pervious concrete

The use of durable, non-chemical, pure, clay-free stone is useful for producing high-quality, durable PC (ACI-552R, 2010); in addition, aggregates must be completely saturated with a dry surface, thus preventing the absorption of design water

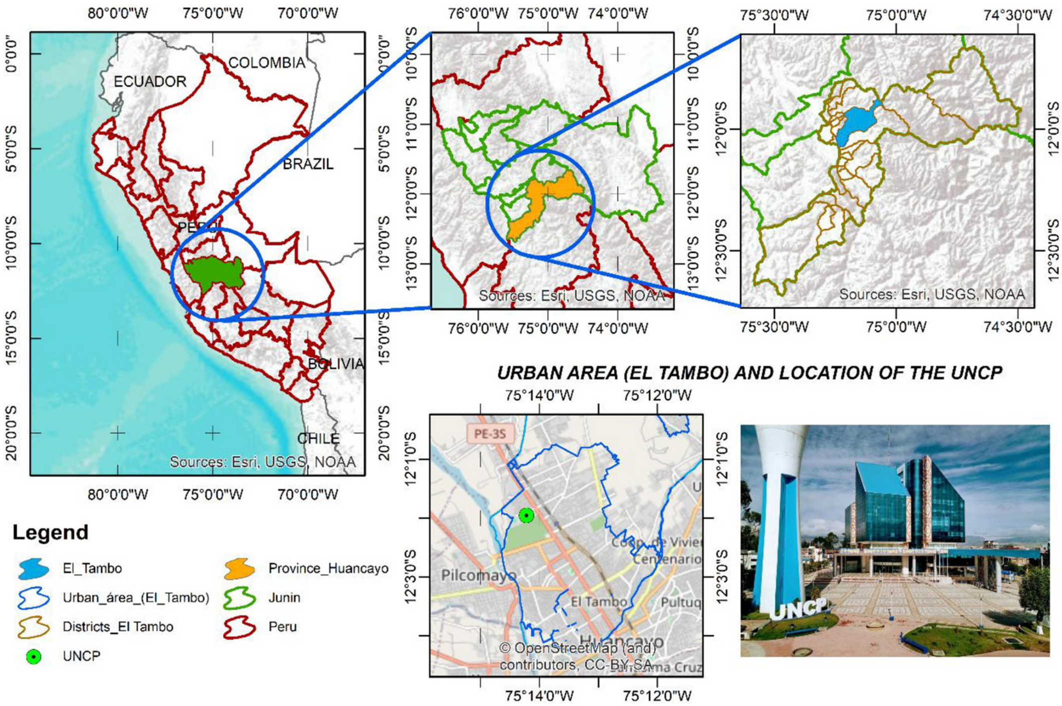


**Figure 1.** Location map of experimental tests on PCs

into the mixture (Mostafa et al., 2024). The use of coarser aggregates with a similar diameter (Elango and Revathi, 2020) and fine aggregates around 5–7% (Zhong and Wille, 2016), is recommended to improve the durability of the concrete. The ASTM C33/C33M standard was used to determine the particle size of the aggregates and their characteristics (ACI-552R, 2010), and Portland cement type II was used in accordance with the ASTM C150 standard (ASTM C150/C150M, 2015).

## Experimental design

In order to investigate possible cause-effect relationships, the experimental method (Heather, 2013) was used to evaluate the proportions of aggregate, color, and plasticizer additive and compare them with control and comparison groups. Likewise, for the population and sample, all information on thermal conductivity and albedo during the period of time in which the laboratory tests were carried out for 90 test tubes was considered. A 3 × 5 × 2 experimental design with 3 repetitions was taken into account (Table 1).

## Mixture preparation or mixture design

This study used ACI 522R-10 (design of mixes for permeable concrete) (ACI-552R, 2010) as a reference, as well as the optimal mix

**Table 1.** Factors and levels for the experimental design of the PC mixture

| Factor experimental | Level | Code |
|---|---|---|
| Size of coarse aggregate (crushed stone) | Held in the ½″ (12.5 mm) mesh | T1/2 |
| | Held in the 3/8″ (9.5 mm) mesh | T3/8 |
| | Held in mesh No. 4 (4.75 mm) | TN4 |
| Color of concrete | Yellow | Y |
| | White | W |
| | Black | B |
| | Green | G |
| | Conventional | C |
| Plasticizer additive | Without additive | SA |
| | With additive | CA |

**Table 2.** Components for a static permeable concrete design

| Material | Weight (1 m$^3$) | Specific gravity (g/cm$^3$) | Absolute volume (m$^3$) | Uniform design (kg) |
|---|---|---|---|---|
| Cement | 413 | 3.12 | 0.132 | 1.00 |
| Water | 124 | 1.00 | 0.124 | 0.30 |
| Stone | 1466 | 2.63 | 0.557 | 3.55 |
| Air void (%) | -- | -- | 0.100 | -- |
| TOTAL | 2003 | -- | 0.910 | -- |

**Table 3.** Components for a dynamic permeable concrete design

| Material | Weight (1 m$^3$) | Uniform design (kg) | Approximate value of a bag (kg) |
|---|---|---|---|
| Cement | 413 | 1.00 | 42.50 |
| Water | 132 | 0.32 | 13.56 |
| Stone | 1490 | 3.61 | 153.33 |
| Air void (%) | 0.15 | -- | -- |
| TOTAL | 2035 | -- | 209.58 |

**Table 4.** Components for the preparation (mixing) of permeable concrete test specimens

| Component | With additive for 3 test tubes | Without additive for 5 test tubes |
|---|---|---|
| Cement (kg) | 2.855 | 3.682 |
| Water (L) | 0.911 | 1.174 |
| Stone (kg) | 9.765 | 12.592 |
| Sand (kg) | 1.085 | 1.399 |
| Additive (ml) | 16.796 | -- |
| Ochre (g) | 142.5 | 245 |

range determined by Adresi et al. (2024) with a cement content of 280 to 310 kg/m$^3$ with certain modifications according to the conditions in Huancayo, a water-cement ratio of 0.27–0.33, an aggregate-cement ratio of 4:1–4.5:1, and a compaction energy level of 18–32 s according to the VeBe test. On the other hand, to determine the compressive strength, the indications of standard NTP 339.034 were considered, so the cylindrical test specimens were subjected to this test at 7, 14, and 28 days of curing (NTP 339-034, 2015).

## Phases of experimentation

Phase I represents the preparation of the PC and examination of the characteristics of the components for testing, for the development of the physical model of the PC system. During this phase, the test specimens were constructed (including the experimental factors in Table 1, with three repetitions), using the optimal mixture design derived from the research by Adresi et al. (2024) and adapted for this study. The ASTM C1170 technical standard was used, the mixture was poured into a 40 cm high container, and the VeBe apparatus was used for 80 s. This process resulted in 90 test specimens 20 cm in diameter and 30 cm in height. The physical model was obtained after 28 days of curing (Figure 2). Figure 2 shows the samples obtained at this stage.

Phase II focused on measuring the performance of the physical PC model with respect to thermal conductivity, thermal resistance, and albedo. The TLS-100 (Figure 3) was used, a portable thermal conductivity meter used to measure thermal conductivity and thermal resistivity, equipped with a 100 mm sensor for testing soils, polymers, and other soft materials. An optional 50 mm sensor has been designed to test harder materials such as rock and concrete. In addition, a pyranometer was used for albedo evaluation. The collected data is automatically analyzed and the results are displayed instantly.

**Figure 2.** View of the permeable concrete test tubes designed in this study

**Figure 3.** Thermtest TLS-100 conductivity and thermal resistance measurement equipment

## Data analysis

The RStudio statistical package (Version 2024.04.2 Build 764) was used for the processing and analysis of the experimental data obtained from the measurements of the 90 permeable concrete (PC) test tubes. Descriptive statistics, normality tests (Shapiro-Wilk), homoscedasticity (Levene's test), multicollinearity (VIF), and three-way factorial analysis of variance were included to evaluate the main effects and interactions of the factors: aggregate size (T1/2, TN4, T3/8), color (Y, W, B, G, C), and plasticizing additive (SA, CA). (Y, W, B, G, C), and plasticizing additive (SA, CA). In addition, it was complemented by a multivariate analysis with interaction graphs, boxplots of significant effects, and a principal component analysis (PCA) to explore the structure of the response variables: thermal conductivity (W/mK), thermal resistance (mK/W), and albedo (%).

# RESULTS

Table 5 shows the overall descriptive statistics for the variables studied, considering all factor values, in which the variability and differentiated distribution are due to the experimental combinations. Thermal conductivity has a high coefficient of variation (CV = 76.676%), reflecting sensitivity to porosity induced by factors; positive asymmetry and high kurtosis suggest that certain treatments generate increases and subgroups of low conductivity (greater insulation), probably associated with a lower number of voids. The case of thermal resistance (CV = 186.395%) indicates that it was the most affected variable, which, together with its leptokurtic kurtosis and wide range, suggests that there are some improvements in the insulating capacity of porous systems compared to conventional ones. On the other hand, albedo (CV = 17.044%) shows considerable symmetry, suggesting that surface reflectance may be related to macroscopic optical properties (color and surface texture).

**Table 5.** Descriptive statistics of the physical PC model

| Variable | N | $\bar{x}$ ± | Median | TM | MAD | Min | Max | Skewness | Kurtosis | SE |
|---|---|---|---|---|---|---|---|---|---|---|
| Thermal conductivity (W/mK) | 90 | 0.057 ± 0.044 | 0.047 | 0.050 | 0.030 | 0.002 | 0.229 | 1.683 | 3.665 | 0.005 |
| Thermal resistance (mk/W) | 90 | 44.365 ± 82.694 | 21.286 | 25.293 | 13.015 | 4.366 | 500 | 4.301 | 19.374 | 8.717 |
| Albedo (%) | 90 | 56.176 ± 9.574 | 57.345 | 56.309 | 9.859 | 38.8 | 75.32 | -0.231 | -0.960 | 1.009 |

**Note:** $\bar{x}$ – mean; $\sigma$ – standard deviation; TM – trimmed mean; MAD – median absolute deviation; SE – standard error.

The Shapiro-Wilk normality test was performed, yielding results for thermal conductivity (p = 7.434e-8), thermal resistance (p = 3.2594e-17), and albedo (p = 0.003). Although the assumption was not met, the design is balanced with a sufficient sample size, in accordance with the principle of the central limit theorem. Furthermore, ANOVA analyses can be continued despite not meeting normality, unless homoscedasticity, independence of factors, and similar sample sizes are met (Knief and Forstmeier, 2021). Levene's test for thermal conductivity (p = 0.908), thermal resistance (p = 0.338), and albedo (p = 0.913) shows that there is statistical homogeneity of variances. The multicollinearity test, evaluated with the variance inflation factor (VIF) for thermal conductivity (VIF = 3.162), thermal resistance (VIF = 1.732), and albedo (VIP = 1.458), thus confirming the independence of factors. The ANOVA indicates that the physical mechanisms of each property are different and that the optimization of the materials has affected optical responses (albedo), since thermal conductivity had low sensitivity and no effects, while thermal resistance had selective effects associated with color and the plasticizer additive. Table 6 indicates that there were no statistically significant effects, although the effects of color ($\eta^2 = 0.1356$) and the interaction of aggregate size x color ($\eta^2 = 0.160$) suggest some influence, but more samples are needed to verify the result.

Table 7 indicates that there are significant effects, with color and interaction with the plasticizing additive having the greatest influence on the resulting physical model. The additive can influence thermal resistance, microstructural changes, and internal porosity, causing certain effects.

Table 8 shows that the color with interactions with other materials has a certain impact on surface reflectance, suggesting that it depends not only on the pigment, but also on the physical arrangement of the granular system and the presence of the additive, as these modify its texture.

Based on the significant interactions, boxplots were created for each one (Figure 4). There is a marginal association between conductivity and

**Table 6.** ANOVA for thermal conductivity (W/mK) of the physical model of the PC

| Parameter | Df | SC | MS | F-value | p-value | $\eta^2$ |
|---|---|---|---|---|---|---|
| Aggregate size | 2 | 0.0001 | 7.078e-05 | 0.0406 | 0.9602 | 0.0014 |
| Color | 4 | 0.0164 | 0.0041 | 2.3540 | 0.0639 | 0.1356 |
| Plasticizer additive | 1 | 0.0000 | 4.817e-05 | 0.0277 | 0.8685 | 0.0005 |
| Aggregate size × Color | 8 | 0.0199 | 0.0025 | 1.4281 | 0.2036 | 0.1600 |
| Aggregate size × Plasticizer additive | 2 | 0.0015 | 0.0007 | 0.4242 | 0.6562 | 0.0139 |
| Color × Plasticizer additive | 4 | 0.0029 | 0.0007 | 0.4132 | 0.7984 | 0.0268 |
| Aggregate size × Color × Plasticizer additive | 8 | 0.0070 | 0.0009 | 0.5051 | 0.8477 | 0.0631 |
| Error | 60 | 0.1045 | 0.0017 | | | |
| Total | 89 | 0.1524 | | | | |

**Note:** DF – degrees of freedom; SC – sum of squares type III; MS – mean square; $\eta^2$ – effect size.

**Table 7.** ANOVA for thermal resistance (mK/W) of the physical model of the PC.

| Parameter | Df | SC | MS | F-value | p-value | $\eta^2$ |
|---|---|---|---|---|---|---|
| Aggregate size | 2 | 23.36 | 11.68 | 0.0018 | 0.9982 | 6.06e-05 |
| Color | 4 | 71878.16 | 17969.54 | 2.7981 | 0.0338 | 0.1572 |
| Plasticizer additive | 1 | 46.28 | 46.28 | 0.0072 | 0.9326 | 0.0001 |
| Aggregate size × Color | 8 | 44696.93 | 5587.12 | 0.8700 | 0.5467 | 0.1039 |
| Aggregate size × Plasticizer additive | 2 | 7081.55 | 3540.77 | 0.5514 | 0.5791 | 0.0180 |
| Color × Plasticizer additive | 4 | 73738.81 | 18434.70 | 2.8706 | 0.0304 | 0.1606 |
| Aggregate size × Color × Plasticizer additive | 8 | 76254.64 | 9531.83 | 1.4843 | 0.1821 | 0.1652 |
| Error | 60 | 385316.25 | 6421.94 | | | |
| Total | 89 | 659035.98 | | | | |

**Note:** DF – degrees of freedom; SC – sum of squares type III; MS – mean square; $\eta^2$ – effect size.

**Table 8.** ANOVA for albedo (%) of the physical model of the PC

| Parameter | Df | SC | MS | F-value | p-value | η² |
|---|---|---|---|---|---|---|
| Aggregate size | 2 | 2.8435 | 1.4217 | 0.1468 | 0.8638 | 0.0049 |
| Color | 4 | 1528.8613 | 382.2153 | 39.4670 | 3.59E-16 | 0.7246 |
| Plasticizer additive | 1 | 0.0580 | 0.0580 | 0.0060 | 0.9386 | 9.98E-05 |
| Aggregate size × Color | 8 | 535.6166 | 66.9521 | 6.9134 | 2.06e-6 | 0.4796 |
| Aggregate size × Plasticizer additive | 2 | 25.5569 | 12.7784 | 1.3195 | 0.2749 | 0.0421 |
| Color × Plasticizer additive | 4 | 123.0552 | 30.7638 | 3.1766 | 0.0196 | 0.1748 |
| Aggregate size x Color × Plasticizer additive | 8 | 208.3470 | 26.0434 | 2.6892 | 0.0135 | 0.2639 |
| Error | 60 | 581.0656 | 9.6844 | | | |
| Total | 89 | 3005.4042 | | | | |

**Note:** DF = Degrees of freedom; SC = Sum of squares type III; MS =Mean square; $\eta^2$ = Effect size.

aggregate size, where fine aggregates (TN4) exhibit greater dispersion and higher mean values, indicating greater heat transfer due to reduced effective porosity in the PC matrix (Figure 4a). In the case of the color-additive interaction with strength, light colors (W, Y) with additive increase the median strength, suggesting a synergistic role in internal thermal dispersion due to microstructural modification (Figure 4b). Albedo, on the other hand, has outliers in pigmented configurations that imply surface variability depending on the formulation (Figure 4c), while color confirms its dominance in the albedo effect (Figure 4d).

The interactions of factors with variable responses (Figure 5) are bivariate and trivialized. Panels (a-c) show low stability in response to factorial variations in conductivity; (d-f) show elevations with plasticizer additive

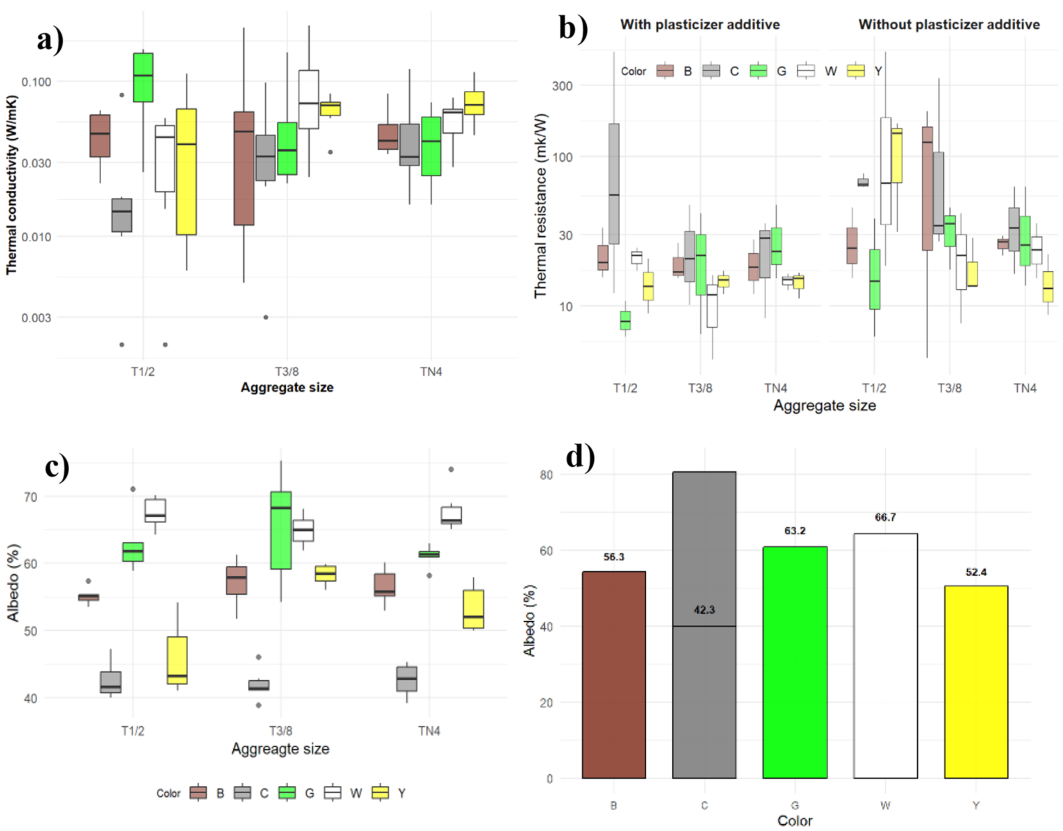


**Figure 4.** Graphs of significant interactions of, a) boxplot of thermal conductivity (W/mK) with size ($p = 0.0494$), b) boxplot of three-way thermal resistance (mK/W) ($p = 0.0304$), c) boxplot of two-way albedo ($p<0.0001$), and d) bar chart of the main effect of albedo with color

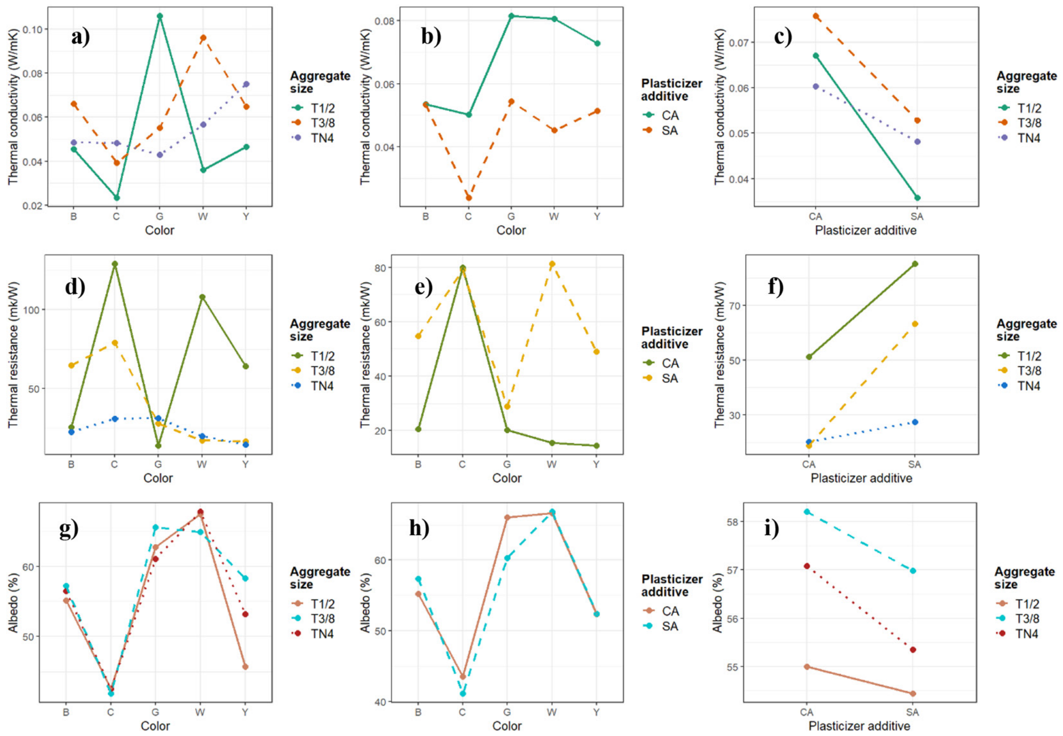


**Figure 5.** Interaction graph of thermal conductivity (a, b, c), thermal resistance (d, e, f), and albedo (g, h, i)

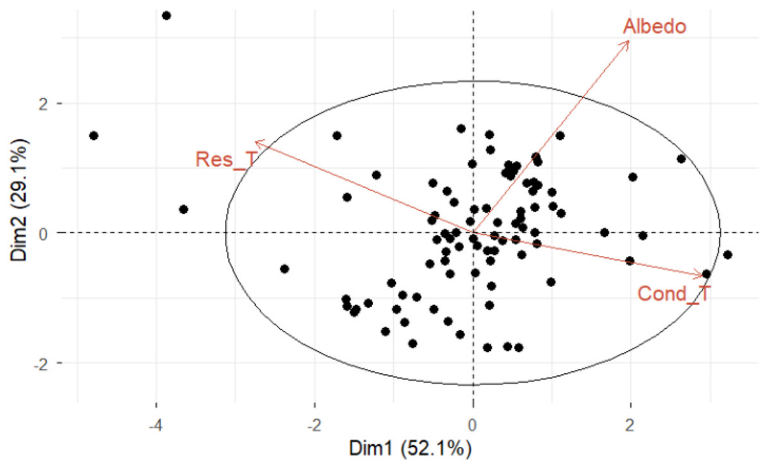


**Figure 6.** Principal component analysis of thermal conductivity (Cond_T), thermal resistance (Res_T), and albedo

and unconventional colors for resistance; (g-i) for albedo, size T3/8 with light pigments maximizes reflectance, suggesting an alternative for UHI mitigation.

Furthermore, in the ACP biplot (Figure 6), it projects the three response variables, where the first component (Dim1) has the highest variance, with an inverse relationship between thermal conductivity and thermal resistance, which shows that heat transport is affected by the structure of the PC. The second component (Dim2) is related to albedo behavior dominated by the optical characteristics of the surface. However, the positive loads of albedo and Rest_T indicate that reflective optimizations co-vary with thermal insulation, while Con_T is linked to aggregate density.

## DISCUSSION

The results highlight the impact of aggregate size on thermal conductivity. The study by

Leyton-Vergara et al. (2019) demonstrated that aggregate particle size affects density, compressive strength, thermal conductivity, and water absorption, which control the thermal behavior of the material. According to the results, low values were obtained, between 0.002–0.229, unlike Sengul et al. (2011), who obtained 0.13–0.35, where fine aggregates can generate this effect in conjunction with other materials that may constitute the mixture, while Arenas et al. (2018) obtained higher values between 0.29–1.02 because it contains recycled concrete and ash aggregates for the production of PC. In addition, with high thermal conductivity, the maximum surface temperature can be reduced by 1–3 °C compared to conventional concrete and heat emission can be reduced by 2.5–5.2% (Chen et al., 2019). Similar to this parameter, thermal resistance increases with porosity (Seifeddine et al., 2022; Singh et al., 2020).

The pore matrix affects heat transfer, so the mixing ratios are more closely related to the thermal properties of PC (Lyu et al., 2024), including permeability, mechanical strength (Ximenes et al., 2022), and thermal storage in pavement (Yaghmour et al., 2024). For this reason, surface temperature variations differ due to their microstructural components, so increasing the thermal conductivity of PC causes its surface temperature to decrease during the day but increase at night, as demonstrated by some studies (Seifeddine et al., 2022). The albedo of PC at the end of 28 days shows a decrease with increasing porosity, which coincides with the work of Lu et al. (2023), who demonstrated that the spectral reflectance of fresh dry PC has the same trend with variations of 0.10–0.35, which is higher than conventional concrete; while Zhang et al. (2015) obtained 0.25–0.35, which can increase solar radiation absorption in the pavement. In addition, 15–35% reduces thermal storage in asphalt (Mostafa et al., 2024). However, for its implementation on roads, certain aspects must be considered, such as the type of traffic, sidewalks, bike lanes, or urban squares (Yaghmour et al., 2025).

Permeable pavements are an environmentally friendly option for reducing the effects of UHI, as some studies have shown that they can produce evaporative cooling due to water storage in the pores (Haddad et al., 2023; Mostafa et al., 2024); Other studies have shown that evaporation can reduce surface temperature by up to 9.4% compared to conventional pavements (Y. Liu et al., 2020). Therefore, it has strategic value for urban climate adaptation, but research on long-term durability, the integration of smart technologies, and advanced obstruction control is needed (Wu et al., 2025). The daytime temperature range must also be considered when evaluating pavement performance, as discovered in Sen et al. (2022).

Therefore, Seifeddine et al. (2022) recommend avoiding the use of lightweight aggregates, favoring fine aggregates with light colors to increase albedo; however, this combination may be limited by the hydraulic properties of PC due to its open porosity. On the other hand, for future studies, the use of PC provides heat relief, reduces emissions, and conserves energy, making it a promising option for environmentally friendly PC road construction (Singh et al., 2020).

## CONCLUSIONS

Thermal conductivity showed low sensitivity to the factors evaluated, with no statistically significant effects found in the ANOVA analysis. However, variations were noted that were mainly related to aggregate size, suggesting that the porous structure and void distribution of PC have an impact on heat transfer within the material matrix.

In contrast, thermal resistance showed statistically significant effects related to concrete color and the interaction between color and plasticizer additive. These findings suggest that certain combinations of pigments and additives can alter the microstructure of the material, improving its thermal insulation capacity.

Surface albedo was the variable that responded most to the experimental factors. The color of the concrete, together with its interactions with aggregate size and plasticizer additive, had a significant impact on surface reflectance. Light-colored mixtures showed higher albedo values, indicating a greater ability to reflect solar radiation and, therefore, less heat storage in the pavement.

Overall, these findings indicate that using permeable pavements can reduce the effects of UHI, but other approaches should be considered to contrast the initial idea, such as durability in everyday environments, evaluation of physical characteristics, and integration of other complementary technologies. Future research should focus on how to increase the albedo of these pavements and on developing effective strategies to combat the urban heat island effect.

## Acknowledgements

To the Universidad Nacional del Centro del Perú for the funded project "Material particulado y condiciones meteorológicas en vías asfaltadas y no asfaltadas en la provincia de Huancayo".


## REFERENCES


1. Abedrabboh, O., Alfarra, M. R., Al-Ansari, T., Fountoukis, C. (2025). Enhancing human thermal comfort in hot arid cities: A systematic review of urban heat island observations and mitigation strategies. *Building and Environment*, *283*, 113398. https://doi.org/10.1016/J.BUILDENV.2025.113398
2. ACI-552R. (2010). *Report on Pervious Concrete*. American Concrete Institute, ACI 522R-10.
3. Adresi, M., Yamani, A., Tabarestani, M. K., Nalon, G. H. (2024). A prediction model for the unconfined compressive strength of pervious concrete based on mix design and compaction energy variables using the response surface methodology. *Buildings 14,* 2834. https://doi.org/10.3390/buildings14092834
4. Ahmed, S. (2018). Assessment of urban heat islands and impact of climate change on socioeconomic over Suez Governorate using remote sensing and GIS techniques. *The Egyptian Journal of Remote Sensing and Space Science*, *21*(1), 15–25. https://doi.org/10.1016/J.EJRS.2017.08.001
5. Alighardashi, A., Mehrani, M. J., Ramezanianpour, A. M. (2018). Pervious concrete reactive barrier containing nano-silica for nitrate removal from contaminated water. *Environmental Science and Pollution Research*, *25*(29), 29481–29492. https://doi.org/10.1007/s11356-018-3008-9
6. AlShareedah, O. S. (2020). *Numerical Modeling of Pervious Concrete for Optimizing Mixture Design and Pavement Thickness* [Washington State University]. https://www.proquest.com/openview/e035569c9e26e6f8a7234f36b7fcb737/1?pq-origsite=gscholar&cbl=18750&diss=y
7. Angeles, S. J., Flores, R. J., Abi, K. H., Mallma, A. G., Angeles, V. R. (2019). Isla de calor urbana superficial en las áreas metropolitanas de Huancayo y Arequipa/Perú. *Anuário do Instituto de Geociências*, *42*(2), 197–207. https://doi.org/10.11137/2019_2_197_207
8. Angeles, V. R., Angeles, S. J., Flores, R. J., Boza, C. F., Angeles, S. N., Suarez, S. L., Abi, K. H. (2024). Urban heat island and increase in temperature on urban roads in Huancayo/Peru[Isla de calor urbano e incremento de temperatura en vias urbanas en Huancayo/Perú]. *Proceedings of the LACCEI international Multi-conference for Engineering, Education and Technology*. https://doi.org/10.18687/LACCEI2024.1.1.192
9. Arenas, C., Leiva, C., Vilches, L. F., Cifuentes, H. (2018). mechanical properties, thermal conductivity, and sound absorption of pervious concrete containing recycled concrete and bottom ash aggregates. *KSCE Journal of Civil Engineering*, *22*(4), 1369–1376. https://doi.org/10.1016/j.wasman.2013.07.008
10. ASTM C150/C150M. (2015). *Standard specification for portland cement*. ASTM Int, vol. 04 (Reapproved).
11. Bai, Y., Xing, Y. (2025). Harnessing green infrastructure for urban heat island mitigation: Evidence-based strategies for sustainable and climate-resilient cities. *Sustainable Cities and Society*, *133*, 106843. https://doi.org/10.1016/J.SCS.2025.106843
12. Bechtel, B., Demuzere, M., Mills, G., Zhan, W., Sismanidis, P., Small, C., Voogt, J. (2019). SUHI analysis using Local Climate Zones—A comparison of 50 cities. *Urban Climate*, *28*, 100451. https://doi.org/10.1016/J.UCLIM.2019.01.005
13. Chandrappa, A. K., Biligiri, K. P. (2016). Pervious concrete as a sustainable pavement material-Research findings and future prospects: A state-of-the-art review. *Construction and Building Materials*, *111*, 262–274. https://doi.org/10.1016/j.conbuildmat.2016.02.054
14. Chen, J., Chu, R., Wang, H., Zhang, L., Chen, X., Du, Y. (2019). Alleviating urban heat island effect using high-conductivity permeable concrete pavement. *Journal of Cleaner Production*, *237*(6), 117722. https://doi.org/10.1016/j.jclepro.2019.117722
15. Cimolai, C., Aguilar, E. (2025). Urban heat hotspots in Tarragona: LCZ-based remote sensing assessment during heatwaves. *Atmosphere, 16*(11), 1283. https://doi.org/10.3390/ATMOS16111283
16. Cleland, S. E., Steinhardt, W., Neas, L. M., Jason West, J., Rappold, A. G. (2023). Urban heat island impacts on heat-related cardiovascular morbidity: A time series analysis of older adults in US metropolitan areas. *Environment International*, *178*, 108005. https://doi.org/10.1016/J.ENVINT.2023.108005
17. Eisenberg, B., Collins, K., Smith, D. (2015). Permeable Paviments. *The American Society of Civil Engineers.* https://doi.org/https://doi.org/10.1061/9780784413784
18. Elango, K. S., Revathi, V. (2020). Mechanical and durability studies on pervious concrete using different types of binders. *Revista Romana de Materiale/ Romanian Journal of Materials*, *50*(2), 258–267. https://www.scopus.com/pages/publications/85090726612
19. Haddad, B., Karaky, H., Boutouil, M., Boudart, B., Sebaibi, N. (2023). Investigation properties of pervious and water-retaining recycled concrete to

mitigate urban heat island phenomena. *Sustainability, 15*(6), 5384. https://doi.org/10.3390/su15065384

20. Heather, S.-R. (2013). A journal paper. *Writing for Science and Engineering*, 83–109. https://doi.org/10.1016/b978-0-08-098285-4.00006-6
21. Joshi, T., Machchhoya, J., Dave, U., Costel, P., Shah, V. (2025). Mitigating urban heat island effects through thermally efficient concrete paver blocks for sustainable infrastructure. *Infrastructures, 11*(1), 5. https://doi.org/10.3390/INFRASTRUCTURES11010005
22. Kevern, J. T., Schaefer, V. R., Wang, K. (2009). *Desing of Pervious Concrete Mixtures* (3° ed). National Pervious Concrete Pavement Association. https://www.researchgate.net/profile/John-Kevern/publication/237654465_Design_of_Pervious_Concrete_Mixtures/links/59ee09de0f7e9b369575907f/Design-of-Pervious-Concrete-Mixtures.pdf
23. Kubilay, A., Derome, D., Carmeliet, J. (2018). Coupling of physical phenomena in urban microclimate: A model integrating air flow, wind-driven rain, radiation and transport in building materials. *Urban Climate*, *24*, 398–418. https://doi.org/10.1016/J.UCLIM.2017.04.012
24. Lai, D., Liu, W., Gan, T., Liu, K., Chen, Q. (2019). A review of mitigating strategies to improve the thermal environment and thermal comfort in urban outdoor spaces. *Science of The Total Environment*, *661*, 337–353. https://doi.org/10.1016/J.SCITOTENV.2019.01.062
25. Leyton-Vergara, M., Pérez-Fargallo, A., Pulido-Arcas, J., Cárdenas-Triviño, G., Piggot-Navarrete, J. (2019). Influence of Granulometry on Thermal and Mechanical Properties of Cement Mortars Containing Expanded Perlite as a Lightweight Aggregate. *Materials, 12*(23), 4013. https://doi.org/10.3390/ma12234013
26. Liu, C., Zhu, C., Bai, G., Quan, Z., Wu, J. (2019). Experimental investigation on compressive properties and carbon emission assessment of concrete hollow block masonry incorporating recycled concrete aggregates. *Applied Sciences, 9*(22), 4870. https://doi.org/10.3390/APP9224870
27. Liu, Y., Li, T., Yu, L. (2020). Urban heat island mitigation and hydrology performance of innovative permeable pavement: A pilot-scale study. *Journal of Cleaner Production*, *244*. https://doi.org/10.1016/j.jclepro.2019.118938
28. Lu, Y., Qin, Y., Huang, C., Pang, X. (2023). Albedo of pervious concrete and its implications for mitigating urban heat island. *Sustainability, 15*(10), 8222. https://doi.org/10.3390/SU15108222
29. Lyu, Q., Dai, P., Chen, A. (2024). Correlations among physical properties of pervious concrete with different aggregate sizes and mix proportions. *Road Materials and Pavement Design*, *25*(12), 2747–2771. https://doi.org/10.1080/14680629.2024.2331193
30. Mirabi, E., Davies, P. J. (2022). A systematic review investigating linear infrastructure effects on Urban Heat Island (UHIULI) and its interaction with UHI typologies. *Urban Climate*, *45*, 101261. https://doi.org/10.1016/J.UCLIM.2022.101261
31. Mostafa, A., Ali, R. Y., Mojtaba, K. T. (2024). Evaluating the effectiveness of innovative pervious concrete pavement system for mitigating urban heat island effects, de-icing, and de-clogging. *Construction and Building Materials*, *449*(3), 138361. https://doi.org/10.3390/buildings11030093
32. NTP 339-034. (2015). Concrete: Standard Test Method for Comprenssive Strenght of Cylindrical Concrete Specimens. *4 ed. Instituto Nacional de Calidad (INACAL)*.
33. Rahmani, N., Sharifi, A. (2025). Urban heat dynamics in Local Climate Zones (LCZs): A systematic review. *Building and Environment*, *267*, 112225. https://doi.org/10.1016/J.BUILDENV.2024.112225
34. Sankar, V. R., John, M., Biswas, W., Sarker, P. (2021). Combating urban heat island effect – A review of reflective pavements and tree shading strategies. *Buildings, 11*(3), 93. https://doi.org/10.3390/BUILDINGS11030093
35. Seifeddine, K., Amziane, S., Toussaint, E. (2022). Thermal behavior of pervious concrete in dry conditions. *Construction and Building Materials*, *345*, 128300. https://doi.org/10.1016/j.conbuildmat.2022.128300
36. Sen, S., Li, H., Khazanovich, L. (2022). Effect of climate change and urban heat islands on the deterioration of concrete roads. *Results in Engineering*, *16*(9), 100736. https://doi.org/10.1016/j.rineng.2022.100736
37. Sengul, O., Azizi, S., Karaosmanoglu, F., Tasdemir, M. A. (2011). Effect of expanded perlite on the mechanical properties and thermal conductivity of lightweight concrete. *Energy and Buildings*, *43*(2–3), 671–676. https://doi.org/10.1016/j.enbuild.2010.11.008
38. Sharifi, A. (2019). Urban form resilience: A meso-scale analysis. *Cities*, *93*, 238–252. https://doi.org/10.1016/J.CITIES.2019.05.010
39. Singh, A., Sampath, P. V., Biligiri, K. P. (2020). A review of sustainable pervious concrete systems: Emphasis on clogging, material characterization, and environmental aspects. *Construction and Building Materials*, *261*, 120491. https://doi.org/10.1016/j.conbuildmat.2020.120491
40. Tun, K. Z., Pramanik, M., Mallick, S. K., Chakraborty, R., Halder, B., Moharir, K. N., Pande, C. B., Zhran, M. (2025). Cooling the cities: A comprehensive review of urban heat island mitigation strategies in Southeast Asia. *Human Settlements and Sustainability*, *1*(2), 91–102. https://doi.org/10.1016/J.HSSUST.2025.05.002

41. Tyson, S., Tayabji, S. (2012). Pervious Concrete [TechBrief]. *United States. Federal Highway Administration*, (FHWA-HIF-13-006). https://doi.org/10.21949/1503647
42. Van, L. (2025). Assessment of the surface urban heat island in Ho Chi Minh City using remote sensing and geographic information systems. *Asian Journal of Water, Environment and Pollution, 22*(6), 210–220. https://doi.org/10.36922/AJWEP025260210
43. Venter, Z. S., Chakraborty, T., Lee, X. (2021). Crowdsourced air temperatures contrast satellite measures of the urban heat island and its mechanisms. *Science Advances*, *7*(22). https://doi.org/10.1126/sciadv.abb9569
44. Wang, R., Luo, W., Liu, Z., Liu, W., Liu, C., Liu, X., Zhu, H., Li, R., Song, J., Hu, X., Han, S., Qiu, W. (2021). Integration of the Extreme Gradient Boosting model with electronic health records to enable the early diagnosis of multiple sclerosis. *Multiple Sclerosis and Related Disorders*, *47*, 102632. https://doi.org/10.1016/J.MSARD.2020.102632
45. Wu, Y., López-Carreño, R. D., Aidarov, S., Álvarez, P. P. (2025). Pervious concrete pavements for climate change adaptation and mitigation: A systematic review of performance, sustainability, and future perspectives. *Road Materials and Pavement Design*. https://doi.org/10.1080/14680629.2025.2544244
46. Xiang, Y., Zheng, B., Bedra, K. B., Ouyang, Q., Liu, J., Zheng, J. (2023). Spatial and seasonal differences between near surface air temperature and land surface temperature for Urban Heat Island effect assessment. *Urban Climate*, *52*, 101745. https://doi.org/10.1016/J.UCLIM.2023.101745
47. Ximenes, J., Jesus, C., Aguiar, J., Pais, J. (2022). Mix design and physical and mechanical properties of pervious concretes. *Materiales de Construcción*, *72*(348), e297–e297. https://doi.org/10.3989/mc.2022.292722
48. Yaghmour, E., Abu Qamar, M., Naito, C., Suleiman, M., Fox, J., Romero, C., Neti, S. (2024). Pressure drop and heat transfer properties for normal weight and lightweight pervious concrete. *Construction and Building Materials*, *425*, 135947. https://doi.org/10.1016/j.conbuildmat.2024.135947
49. Yaghmour, E., Abu Qamar, M., Naito, C., Suleiman, M., Fox, J., Romero, C., Neti, S. (2025). Experimental investigation of the performance of lightweight pervious concrete for pavement applications. *International Journal of Pavement Engineering*, *26*(1). https://doi.org/10.1080/10298436.2025.2531193
50. Zhang, R., Jiang, G., Liang, J. (2015). The Albedo of Pervious Cement Concrete Linearly Decreases with Porosity. *Advances in Materials Science and Engineering*, *2015*(1), 746592. https://doi.org/10.1155/2015/746592
51. Zhong, R., Wille, K. (2016). Compression response of normal and high strength pervious concrete. *Construction and Building Materials*, *109*, 177–187. https://doi.org/10.1016/j.conbuildmat.2016.01.051